Biomaterials Science

ROYAL SOCIETY OF CHEMISTRY

PAPER

View Article Online
View Journal | View Issue

Cite this: *Biomater. Sci.*, 2023, **11**, 2395

Nitric oxide scavengers based on *o*-phenylenediamine for the treatment of rheumatoid arthritis

Yeong Mi Lee,†[a] Sanggi Lee†[a,b] and Won Jong Kim *[a,b]

Nitric oxide (NO) plays various physiologically favorable roles in the body. However, excessive production of NO causes inflammation and leads to various chronic inflammatory diseases. A typical NO-related disease is rheumatoid arthritis (RA), and it is well known that NO is a critical molecule for inflammation in the pathophysiology of RA. Therefore, depletion of NO can be an attractive treatment option for RA. In this study, we proposed a new method to discover effective NO scavengers in the form of small molecules. *o*-Phenylenediamine (*o*-PD), the core structure of the NO scavenger, is a diamino-aromatic compound that irreversibly reacts with NO through nucleophilic substitution of amine. Inspired by the nucleophilicity, we attempted to find new scavenger candidates by searching for conditions that increase the nucleophilicity of the amine moieties. Candidates were classified into the basic form *o*-PD, monoamine aniline, *o*-PD substituted with a nitro group, carboxyl group, and three methyl groups. The NO-scavenging ability of these candidates was demonstrated using the DAF-2 assay. *N*-Methyl-*o*-PD (N-Me) in the methyl ($-CH_3$) group had the highest reactivity with NO among the candidates, and the efficiency of NO scavengers was confirmed *in vitro* and *in vivo*. Depleted levels of NO and reduced levels of pro-inflammatory cytokines by N-Me demonstrated remarkable therapeutic efficacy against joint damage and delayed severity in a collagen-induced arthritis (CIA) model. Therefore, our findings suggest that N-Me is a new NO scavenger with great potential for RA treatment and further clinical drug development.

Received 4th December 2022,
Accepted 4th February 2023

DOI: 10.1039/d2bm01994a

rsc.li/biomaterials-science

1. Introduction

Rheumatoid arthritis (RA) is an inflammatory disease in which the synovial membrane surrounding the joint becomes primarily inflamed, causing swelling of the synovial membrane followed by cartilage loss and bone destruction. Although the etiology remains unclear, the main risk factors inducing inflammation include genetics, infection, and environmental factors.[1] These trigger autoimmune reactions that recognize the body as an enemy, thus causing chronic inflammation to spread throughout the body. As arthritis progresses, joint deformation begins, and the joint loses its function, making it difficult to recover even with treatment.[2] Therefore, it is important to control inflammation in the moderate stages in order to prevent severe joint damage. Owing to this reason, the RA drug market is expected to grow by 1% annually and reach $29.1 billion in 2029, increasing the importance of developing new treatments.[3]

The currently known pathology of RA is that RA is an autoimmune disease, and an abnormality in the immune system is considered to be a critical factor in its pathogenesis. Immune cells activated by an autoimmune reaction infiltrate the joints through blood vessels or tissue-specific pathways,[1,4] and $CD4^+$ T cells and macrophages secrete pro-inflammatory cytokines, nitric oxide (NO), and other substances that induce local inflammation in the joints. This inflammatory environment stimulates synoviocytes constituting the synovial membrane to produce matrix metalloproteinases (MMPs) that degrade cartilage and receptor activator of nuclear factor κB ligand (RANKL), which promotes the differentiation of osteoclasts, leading to the breakdown of bone formation, bone erosion, and joint disorders.[5,6]

Although attempts to directly undermine fundamental autoimmunity have been made, they still have several limitations, including remission and side effects. According to recent standard treatment guidelines, methotrexate (MTX) is administered or injected as first-line treatment. MTX inhibits DNA and RNA synthesis in cells to induce apoptosis and reduces cytokine production by inhibiting COX-2, an enzyme

[a]*Department of Chemistry, Pohang University of Science and Technology (POSTECH), Pohang 37673, Republic of Korea. E-mail: wjkim@postech.ac.kr; Fax: +82-54-279-3399; Tel: +82-54-279-2104*
[b]*School of Interdisciplinary Bioscience and Bioengineering, Pohang University of Science and Technology (POSTECH), Pohang 37673, Republic of Korea*
†These authors contributed equally to this work.

involved in inflammation.[7] MTX treatment is effective in delaying disease progression, but non-specific immune suppression causes substantial side effects, and no therapeutic effect is observed in 30–40% of patients.[8] Patients who have no response to MTX are treated with biological drugs. These include cytokine inhibitors, which directly inhibit pro-inflammatory cytokines, and JAK inhibitors, which block inflammation-related pathways. Cytokine inhibitors have a significant therapeutic effect by directly inhibiting the target molecules. However, in the case of a patient who still has no therapeutic response this treatment should be changed to a biologic or targeted medication in a different cytokine class and re-administration.[9] It also has the disadvantage of being vulnerable to infection by suppressing the corresponding immunity.[10] Therefore, it is urgent to find new treatment targets that play a more critical role in controlling the immune system.

Recently, NO has become an attractive target molecule for the treatment of autoimmune diseases. NO is a free radical molecule synthesized by nitric oxide synthase (NOS) in the process of converting L-arginine to L-citrulline in cells.[11] It has various physiological roles in the body, depending on the concentration of NO. Low concentrations of NO are involved in vasodilation and serve as cellular signal transduction.[12] In contrast, at relatively high concentrations of NO, it is known to be involved in immune regulation and tissue destruction by reacting with reactive oxygen species (ROS).[13,14] NO is also involved in the immune response in RA. Excess endogenous NO promotes the differentiation of effector T cells (*e.g.*, Th1, Th17), a subset of $CD4^+$ T cells involved in inflammation,[15] while helping macrophages to migrate to the site of local inflammation and maintain their activity. Subsequently, the NO-induced immune response results in elevated levels of pro-inflammatory cytokines in the joints.[16,17] When stimulated with an inflammatory response, synoviocytes and chondrocytes located in the joint also produce an excessive quantity of NO, contributing to maintaining a high NO concentration and causing a continuous inflammatory response.[18,19] Chondrocytes become dead by NO-induced apoptosis, leading to cartilage degradation,[20] and the bone homeostasis maintained by the balance of osteoblasts and osteoclasts is disrupted by the influence of RA-exacerbating factors.[21–23] It can even cause joint disorders, making RA more severe. In special, NO is associated with an inflammatory environment. In an inflammatory environment, increased expression of NO synthase (NOS) leads to overproduction of NO, which activates COX-2 to produce increased amounts of PGE_2.[24] Therefore, the depletion of excess NO in RA lesions can alleviate abnormal immune responses, and as a result, the homeostasis of bone formation can be balanced, leading to the recovery of the joint.

In this regard, various NO scavengers have been reported to selectively deplete excess NO. Typical NO scavengers include nitric oxide synthase inhibitors[25,26] and dexamethasone,[27] which inhibit production of endogenous NO, and *o*-Phenylenediamine (*o*-PD)[28] which directly reacts with NO. In our previous studies, in order to remove NO efficiently, we discovered various NO scavengers that are highly reactive to NO. A polymer-structured complex system for depleting NO based on *o*-Phenylenediamine (*o*-PD) was developed.[29,30] The reaction of *o*-PD with NO is initiated by a nucleophilic substitution reaction of the amine in *o*-PD, which forms an intermediate diazonium and then forms a triazole. Through this irreversible reaction of *o*-PD with NO, the level of NO can be reduced efficiently.[31,32] However, for stronger NO-scavenging, the reactivity of the *o*-PD moiety should be precisely tuned. We hypothesize that the reaction of *o*-PD with NO depends on the electron density of *o*-PD, focusing on the nucleophilicity of the lone pair electrons of the nitrogen atom of *o*-PD.[33] Accordingly, we modified *o*-PD with various substituted moieties and investigated the reaction activity with NO. To test this hypothesis, candidates with various substitutions were selected, their relative NO reactivity was evaluated, and the NO scavenger with the highest reactivity was selected. The efficacy of the selected NO scavenger was also evaluated *in vitro* and using an *in vivo* mouse model of RA (Scheme 1).

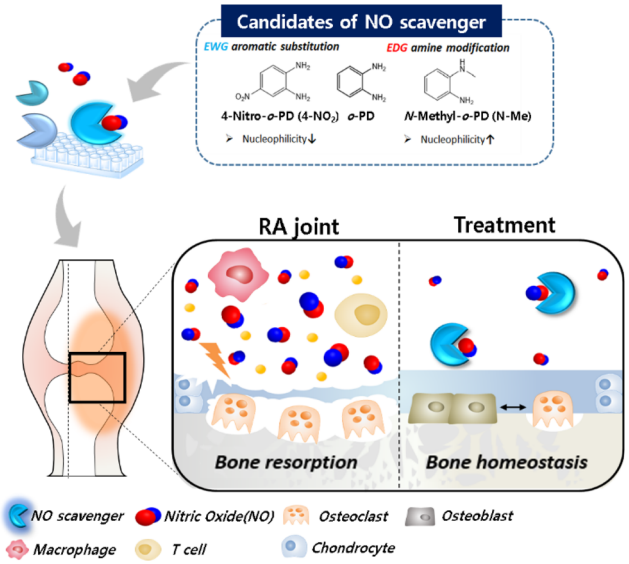

Scheme 1 A schematic illustration of development of drug candidates based on NO-scavenging for rheumatoid arthritis treatment. Drug candidates were selected according to variation in nucleophilicity among *o*-Phenylenediamine (*o*-PD) derivatives. NO-scavenging ability of candidates were investigated using DAF-2 assay, and the candidate with the best NO-scavenging was studied *in vitro* and *in vivo*.

2. Materials and methods

2.1. Reagents

General chemicals were commercially available and used without further purification. Lipopolysaccharide (LPS), collagen type II from chicken sternal cartilage, complete Freund's adjuvant (CFA), incomplete Freund's adjuvant (IFA), thiazolyl blue tetrazolium bromide (MTT), Griess reagent kit and 4,5-Diaminofluorescein (DAF-2) were purchased from Sigma-

Aldrich (St Louis, MO). 4-Amino-5-Methylamino-2′,7′-Difluorofluorescein Diacetate (DAF-FM Diacetate) was purchased from Invitrogen (Carlsbad, CA, USA). ELISA kits for mouse IL-6, TNF-α, and IL-17 were purchased from Koma Biotech (Seoul, Korea). NIH3T3 (murine fibroblast) and RAW 264.7 (murine macrophage) cell lines were purchased from the Korean Cell Line Bank (Korea).

2.2. Instrumentation

Nuclear magnetic resonance of ^{1}H NMR was measured using Bruker Advance 300 MHz and 500 MHz FT-NMR. Fluorescence and absorbance for the MTT assay, Griess assay, and ELISA were measured using a multi-detection microplate reader (Spectramax® i3, Molecular Devices) and analyzed using SoftMax® Pro 6 software. Fluorescence microscopy images were obtained using a Nikon Eclipse Ti-E microscope and analyzed using NIS-Elements software (ver. 4.2). The micro-CT images were scanned using a preclinical PET/SPECT/CT system (Siemens Medical Solutions, PA, USA). The histological assay images were obtained using a microscope (Nikon Eclipse 80i, USA). All data were statistically analyzed using GraphPad Prism 7.

2.3. NO-scavenging ability of *o*-PD derivatives by DAF-2 assay

For the measurement of the scavenging ability of the *o*-PD derivatives, DAF-2 assay was employed. Briefly, general chemicals were dissolved in pure DMSO to achieve a 5 mM stock concentration, and pyNO (NO donor) was dissolved in 1 mM NaOH to achieve a 0.5 mM stock concentration. One microliter of 5 mM DAF-2 in DMSO was added to each e-tube. The prepared *o*-PD derivatives were then added to the e-tubes in the same volume. In the background and DAF-2 only groups, 1 μL of DMSO was added instead of the *o*-PD derivatives. The solutions were then vortexed. Next, 488 μL DPBS was added to each solution. In the background group, 498 μL of DPBS was added to each solution to obtain a total volume of 500 μL. Finally, 10 μL of 0.5 mM pyNO was added to the e-tubes, except in the background group. After incubation for 30 min at room temperature (RT) in the dark, 100 μL aliquots were transferred into 96-well plates. Fluorescence intensity was measured at Ex/Em 495/520 nm, and the relative fluorescence of the DAF-2-only group was regarded as 100%. The reaction ratio of DAF-2 to NO was calculated using the following equation: Reaction ratio of DAF-2 to NO (%) = 100 × (FL of DAF-2 + each sample − FL of background)/(FL of DAF-2 only − FL of background). The time curve was also obtained under the same conditions and was followed by kinetic readings every 5 min for 60 min.

2.4. Confirmation of NO-responsiveness by NMR

N-Methyl-*o*-PD (N-Me) (2 mg, 10.3 μmol) was added to 1 mL of a 100 μM NO solution in distilled water and incubated for 24 h at RT. Subsequently, the samples were lyophilized and dried. For NMR measurements, DMSO was added to the dried sample, and NMR spectra were measured.

2.5. Solubility test

To evaluate solubility, absorption was measured at 300 nm for N-Me, 310 nm for 4-Me, 330 nm for 4-COOH, and 430 nm for 4-NO_2. Each sample was diluted from 50 μg mL^{-1} to 0 μg mL^{-1} to obtain a standard curve.

2.6. Cytotoxicity test

The cytotoxicity of *o*-PD derivatives was evaluated using an MTT assay with NIH3T3 and Raw 264.7 cells. NIH3T3 cells were seeded in 96-well plates at a density of 8×10^3 cells per well in 200 μL DMEM formulated with the addition of 10% FBS, 100 U mL^{-1} penicillin, and 100 μg mL^{-1} streptomycin and incubated for 24 h at 37 °C. The medium was then replaced with fresh medium, and the cells were incubated for 48 h with each sample. Sample preparation was performed in 0.2 M HCl solution for increasing solubility, and added to cell culture media to make the final concentration diluted 1000 times. The medium was removed, washed with DPBS, and incubated with 0.5 mg mL^{-1} of MTT solution in DMEM containing 10% FBS for 4 h. After incubation, the MTT solution was carefully aspirated, and 200 μL of DMSO was added to each well to dissolve the crystal violet. Then, 100 μL aliquots were transferred to a 96-well plate, and the absorbance of the formazan compound was measured at 570 nm using a micro spectrofluorometer (VICTOR 3V Multilabel Plate Counter, PerkinElmer, MA, USA). The relative absorbance of untreated cells was evaluated as 100% viability. Raw 264.7 cells were seeded at a density of 1×10^4 cells per well, and the medium was replaced with fresh medium or medium with 1 μg mL^{-1} of LPS and further proceeded in the same process as described above.

2.7. Fluorescence imaging of intracellular NO in raw 264.7 cells

Intracellular NO detection was carried out using confocal laser scanning microscopy to compare the NO-scavenging ability of the *o*-PD derivatives. Raw 264.7 cells were seeded in 6 well plates at a density of 2×10^5 cells per well in 2 mL DMEM formulated with the addition of 10% FBS, 100 U mL^{-1} penicillin, and 100 μg mL^{-1} streptomycin and incubated overnight at 37 °C. The medium was replaced with fresh medium or medium with 1 μg mL^{-1} of LPS for each sample and incubated for 48 h at 37 °C. After incubation, the medium was removed, and the cells were washed with cold DPBS. Samples were prepared in the same method as cytotoxicity test.

Raw 264.7 cells were further incubated with serum-free medium containing 5 μM DAF-FM DA for 40 min. The cells were then washed with cold DPBS and fixed with 10% neutrally buffered formalin (NBF) with Hoechst 33342 (Thermo Fisher, cat. 62249) for 15 min at RT and immediately viewed by fluorescence microscopy.

2.8. Hemolysis assay

Mouse blood was freshly prepared and diluted 5-folds with PBS, followed by centrifugation at 2000 rpm for 3 min, and the

supernatant was removed to obtain RBCs. RBCs were washed with phosphate-buffered saline (PBS). Then, IC_{50} concentration of N-Me in PBS, Triton X-100 1% (v/v), or PBS was added into RBCs, and the mixed solutions were incubated at 37 °C for 2 h, followed by centrifugation. The absorbance of the supernatant was measured at 541 nm, corresponding to the release of hemoglobin. PBS and Triton X-100 served as the negative (0% hemolysis) and positive controls (100% hemolysis), respectively.

2.9. Animals

All experiments involving animals were approved by the POSTECH Biotech Center Ethics Committee (POSTECH-2021-0016) under guidelines and regulations provided by Postech Institutional Animal Care and Use Committee (IACUC). Male DBA1/J mice (6–8 weeks old; body weight 18–20 g, Jackson Laboratory) were purchased from Orient Bio (Gyeonggi, Korea). The animals were housed in a controlled environment and provided with a standardized rodent diet and water in the animal care facility of the University of POSTECH.

2.10. Establishment of CIA mouse model

To establish the collagen-induced arthritis (CIA) model, an emulsion formulated with 100 μL of collagen (2 mg mL^{-1}) in 0.01 N acetic acid mixed with CFA in a 1 : 1 (v/v) ratio was injected into the tail or intradermally. After 21 days, an emulsion formulated with 100 μL of collagen (2 mg mL^{-1}) in 0.01 N acetic acid mixed with IFA in a 1 : 1 (v/v) ratio was injected.

2.11. *In vivo* efficacy test of N-Me in RA mouse model

The immunized mice were divided into three groups. Treatment was initiated when the CIA mouse showed the first symptoms. MTX and DPBS were chosen as the positive (0.1 mg kg^{-1}) and negative controls, respectively. All samples, including N-Me (100 mg kg^{-1}), were injected intraperitoneally three times per week for two weeks. The drugs and vehicle were administered to CIA mice at a final volume of 100 μL per mouse. Clinical score estimation was conducted with a blind test, and scores on a scale of 0–4 were evaluated for each paw (0: No redness and swelling; 1: Redness and mild swelling confined to the tarsals or 1–2 toes; 2: redness and mild swelling extending from the entire paw or swelling of 3+ toes; 3: severe redness and moderate swelling extending from the ankle to metatarsal joints; 4: severe redness and severe swelling encompassing the ankle, foot, and digits, or ankylosis of the limb).

2.12. *Ex vivo* CT imaging and histology assay

CIA mouse paw samples on day 35 were fixed in 7% formaldehyde overnight and stored in 70% ethanol. Bone and joint morphology were monitored using computed tomography (CT) to determine the degree of bone resorption in each group. For histological analysis, the paws of sample-treated mice were fixed in 7% formaldehyde and decalcified with a decalcifying solution for 7–30 days. Safranin-O and hematoxylin and eosin (H&E) staining were performed according to the manufacturer's protocol.

2.13. Quantification of cytokines and NO level in paw tissue and serum

CIA mouse serum and paw samples were collected on day 35, and the concentrations of TNF-α, IL-6, and IL-17 in the serum and paw tissue were quantified using ELISA according to the manufacturer's protocol. Serum was prepared by centrifugation at 3000 rpm, 4 °C for 10 min to remove blood clots. Paw tissue was prepared by suspending paw homogenates in cold PBS (500 μL). Then, centrifugation was performed at 13 000 rpm, 4 °C for 30 min to obtain the supernatant. Similarly, paw tissue samples were prepared for the Griess assay, and NO levels were measured according to the nitrite kit protocol.

3. Results and discussion

3.1. Selection of drug candidates with *o*-PD moiety

To search for a more potent NO-scavenger as a therapeutic agent for RA, we evaluated the reactivity of *o*-PD-based candidates with NO. The *o*-PD-based NO scavengers form benzotriazole by reacting with NO, allowing irreversible scavenging.[34,35] It is initiated by the lone pair electrons present on the nitrogen of the amine moiety, and the reactivity of the NO scavenger with NO can be governed by its nucleophilicity. Based on this, the reactivity of the NO scavenger was improved by increasing the electron density of the aromatic primary monoamine.[36,37] Considering this mechanism, it is hypothesized that the reactivity of *o*-PD with NO can be tuned by substituting an electron-donating group (EDG) to increase the electron density by providing electrons. In contrast, electron-withdrawing groups (EWG) are hypothesized to reduce electron density by attracting electrons. Based on the substituent effect, the NO scavengers were classified into the basic form *o*-PD, monoamine aniline, EWG nitro ($-NO_2$), carboxyl (–COOH), and EDG methyl ($-CH_3$) groups. The methyl group was divided into the amine-modified form ($-NHCH_3$) and different aromatic substitutions with *ortho*- or *para*-positions (Fig. 1a).

3.2. NO scavenging ability of the candidates confirmed by DAF-2 assay

The NO-scavenging ability of the six candidates was measured through the relative reactivity with NO using a DAF-2 assay. DAF-2 is a highly sensitive and NO-specific fluorescent probe that reacts with NO to form the fluorescent triazole DAF-2T in the presence of O_2.[38] First, the fluorescence profile of the DAF-2 reagent was monitored after the reaction with NO. The fluorescence intensity of DAF-2T was measured at 5 min intervals for 30 min. A significant increase in fluorescence intensity was observed in the DAF-2 group (DAF-2 + NO) for 10 min, which then plateaued until 30 min (Fig. 1b). In contrast, when *o*-PD derivatives were added, the fluorescence intensities decreased depending on the NO scavenger. The order of the reduced fluorescence was *N*-Methyl-o-PD (N-Me) > 4-Methyl-*o*-PD (4-Me) > 3-Methyl-*o*-PD (3-Me) > 4-Carboxyl-*o*-PD (4-COOH) > Aniline > 4-Nitro-*o*-PD (4-NO_2). The reduced fluorescence was due to the competition of DAF-2 with NO scavengers for the

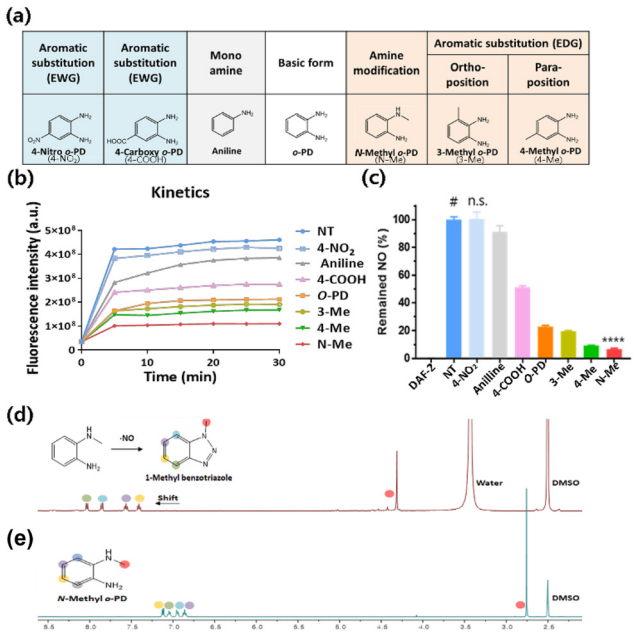

Fig. 1 Nitric oxide (NO)-scavenging ability of *o*-PD derivatives. (a) The 7 drug candidates were selected according to the variation in substitution of *o*-PD base structure. (b) The fluorescence intensity measured for 30 min w/ or w/o *o*-PD derivatives in the reactions of DAF-2 and NO. (c) Remained NO (%) at end point of reaction for 30 min (n = 5, Mean ± SD, # compared to sample groups, t-test, ****p < 0.0001, *DAF-2: Diaminofluorescein-2, *EWG: Electron withdrawing group, *EDG: Electron donating group). (d) NMR measurement for confirmation of benzotriazole formation from *N*-Methyl-*o*-PD (N-Me). (e) ^{1}H NMR spectrum of *N*-Methyl-*o*-PD (N-Me) in DMSO.

reaction with NO. The difference in fluorescence intensity when the six candidates were added might be also owing to the difference in reactivity with NO arising from their electronic properties. The NO-scavenging ability of the candidates was also studied by measuring the fluorescence of the remaining NO in the assay solution after the reaction. The intact fluorescence intensity of DAF-2 was set to 100% of the remaining NO and the NO-scavenging ability of the *o*-PD derivatives was evaluated accordingly. As shown in Fig. 1c, the order of the decrease in the remaining NO (%) was N-Me > 4-Me > 3-Me > 4-COOH > aniline > 4-NO_2, which is consistent with the time course results (Fig. 1b). It was found that N-Me had the highest NO-scavenging ability (>90%), whereas 4-NO_2 was found to have the lowest ability, similar to that of the DAF-2 group. According to these results, *o*-PD substituted with an electron-donating group showed increased reactivity to NO. The methyl-substituted group revealed a higher NO-scavenging effect at the *para* position (4-Me) than at the *ortho* position (3-Me) in the benzene ring,[39] although a detailed study on the mechanism is in progress. This indicates that the electron density of the benzene ring substituted with EDG and the significant electron density of the nitrogen of methyl amine can increase the reactivity of *o*-PD with NO. Therefore, N-Me has the greatest potential to be used as a NO scavenger because it has a higher nucleophilicity than normal amines. When N-Me reacted with NO, the benzotriazole structure was also confirmed using NMR spectroscopy (Fig. 1d and e).

3.3 Drug solubility and cytotoxicity

The solubility of drug compounds plays a critical role in absorption during pharmaceutical drug development.[40] Therefore, to determine the maximum concentrations of N-Me, 4-Me, 4-COOH, and 4-NO_2, a drug solubility test was performed. All candidates were prepared at a concentration of 50 mg mL^{-1}, and solubility test was carried out at pH 3, pH 5, 0.5 M HCl and distilled water (DW). N-Me (HCl form) revealed 40 mg mL^{-1} solubility at pH 3, pH 5, and DW. In contrast, 4-NO_2 showed low solubility at pH 3, pH 5, and DW, whereas the solubility of 4-NO_2 increased over 20 mg mL^{-1} in 0.5 M HCl (Fig. 2a). The order of solubility under acidic conditions is N-Me > 4-Me > 4-COOH > 4-NO_2. Thus, N-Me has high solubility in all solvents, which means that a high dose can be used to maximize the therapeutic effect regardless of the type of administration. The cytotoxicity of the candidates in normal cells was investigated to obtain the IC_{50} (half maximal inhibitory concentration) value, which is correlated with drug potency. The candidates of various concentrations were incubated for 48 h at NIH3T3 cells. Interestingly, the cytotoxicity of methyl amines N-Me and 4-Me was higher than that of both 4-COOH and 4-NO_2 at the same concentration (Fig. 2b and c). N-Me exhibited an IC_{50} value of approximately 47 μM, similar to that of 4-Me (Fig. 2d). The order of the lowest IC_{50} value in NIH3T3 cells was N-Me > 4-Me > 4-NO_2 > 4-COOH.

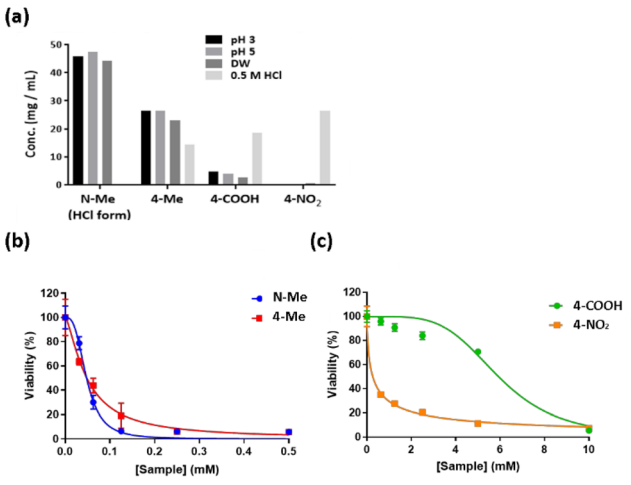

(d)

NIH3T3	N-Me	4-Me	4-COOH	4-NO_2
IC_{50} (μM)	47.83 ± 2.3	48.41 ± 2.4	5933 ± 539	262.5 ± 37.2
LD_{50} (mg/kg)	243	205	1332	416

Fig. 2 Pharmacological properties of the candidates. (a) Drug solubility profile. All samples were prepared at a concentration of 50 mg mL^{-1} and dissolved in solvents with different conditions. (b and c) Cell viability tested in NIH3T3 cells (n = 5, Mean ± SD). (d) IC_{50} value of N-Me, 4-Me, 4-NO_2, and 4-COOH in NIH3T3 cells (n = 5, Mean ± SD).

3.4. NO scavenging ability in cultured cells

Next, the NO-scavenging abilities of the candidates were evaluated *in vitro*. Raw 264.7 cell, a murine macrophage cell line, is known to produce high concentrations of NO by induced Nitric Oxide Synthase (iNOS) when stimulated by a pathogen, such as Lipopolysaccharide (LPS).[41] Raw 264.7 cells were stimulated with LPS (1 μg mL^{-1}), followed by treatment of NO scavengers. We selected N-Me and 4-NO_2 for the study of cell cytotoxicity and NO-scavenging ability in Raw 264.7 cells because N-Me has high drug solubility and high NO-scavenging ability, whereas 4-NO_2 has similar drug solubility but low NO-scavenging ability. As shown in Fig. 3a and b, N-Me showed lower cytotoxicity than 4-NO_2, in both LPS-treated and LPS-non-treated RAW 264.7, while N-Me showed slightly higher cell viability in the LPS-treated cells than the LPS-non-treated cells. To evaluate the NO-scavenging ability, LPS-stimulated RAW 264.7 cells were treated with N-Me or 4-NO_2, and intracellular NO was monitored using fluorescence imaging. As a control, the LPS-untreated cells were also treated with N-Me and 4-NO_2. As shown in Fig. 3c, compared to the LPS-untreated group, the LPS-treated group generated a significant amount of NO, as indicated by increased green fluorescence, confirming that LPS stimulated NO production in Raw 264.7 cells. When treated with N-Me, the fluorescence of NO significantly decreased, whereas the green fluorescence of NO slightly declined when treated with 4-NO_2. This result indicates that N-Me reacts with NO more efficiently than with 4-NO_2; thus, N-Me has potential applications as a NO scavenger under physiological conditions.

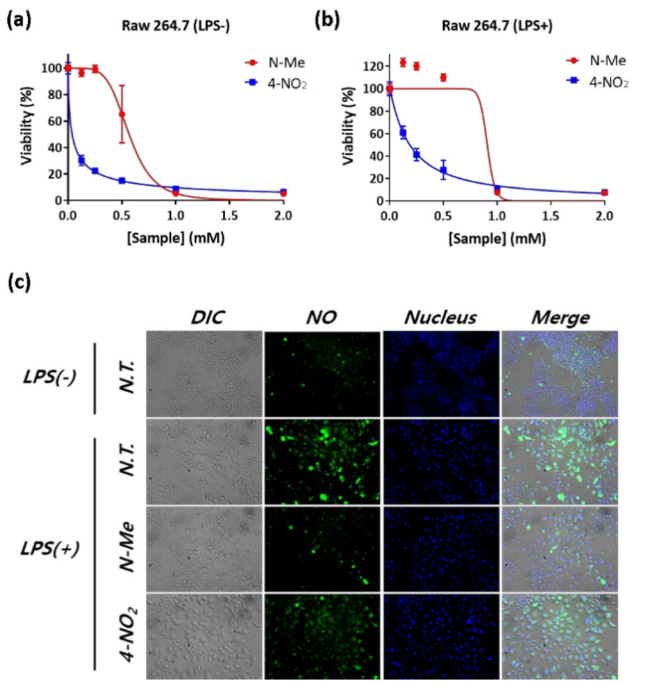

Fig. 3 *In vitro* NO-scavenging ability test of N-Me and 4-NO_2. (a and b) Cytotoxicity profile evaluated in Raw 264.7 cell (n = 5, Mean ± SD). (c) Fluorescence imaging of intracellular NO. The candidates were treated at a concentration of 20 μM (>70% viability against Raw 264.7 cells). DAF-FM-DA: NO (green), Hoechst: Nucleus (blue) (scale bar = 100 μm).

3.5. Cyto- and hemo-compatibility assay of N-Me

As N-Me has good solubility and NO-scavenging ability, we selected N-Me as a potent NO scavenger for further *in vivo* efficacy. Prior to the evaluation of the therapeutic efficacy of N-Me *in vivo*, cyto-and hemo-compatibility tests were conducted because N-Me should be non-toxic when delivered throughout the body since RA is a systemic inflammatory disease. It was tested at a higher or lower concentration based on the IC_{50} value (47.83 μM) for NIH3T3 cells. The viability of NIH3T3 cells was identical to the IC_{50} value (Fig. 4a). N-Me had a hemolytic capacity of only 0.47% in IC_{50} and was negligible even at higher concentrations, confirming that it is suitable for systemic delivery (Fig. 4b).

3.6. Therapeutic efficacy of N-Me in CIA model

Next, we evaluated the therapeutic efficacy using the NO-scavenging activity of N-Me in murine RA models. We employed a CIA model as it is the most common model for arthritis and induces autoimmune response using type II collagen, a major component of cartilage tissue, among autoantigens that cause autoimmunity in human RA.[42] After immunization, mice were randomly divided into three groups: N-Me, PBS, and MTX-treated groups. Each sample was injected into the mice three times a week for a total of two weeks (Fig. 5a). The clinical score was monitored to evaluate the severity of arthritis after sample administration until the 35th day, after which the mice were sacrificed for analysis. As shown in Fig. 5b, the N-Me-treated group had a clinical score similar to that of MTX, a positive control, and showed an enhanced clinical score compared to the PBS group. During monitoring, no change in the weight of the mice was observed, indicating that the drugs are not toxic (Fig. 5c).

3.7. Investigation of bone destruction by CT imaging and histology

It is known that osteoclast differentiation caused by NO-induced inflammation of the RA lesion induces bone resorp-

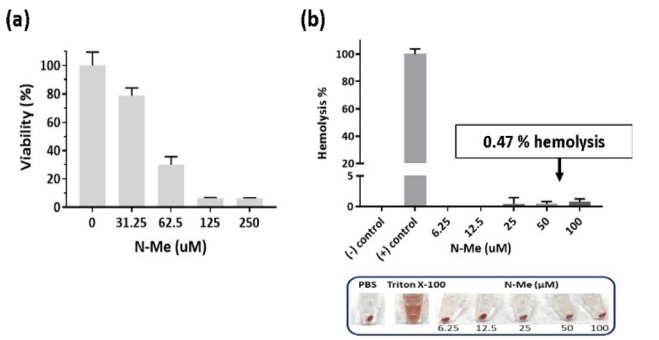

Fig. 4 Cyto/hemo-compatibility of N-Me. (a) Cell viability against NIH3T3 cells (n = 5, Mean ± SD). (b) Hemolysis assay. Mouse whole blood and N-Me were incubated at 37 °C for 2 h. The supernatant was observed at 541 nm (n = 3, Mean ± SD).

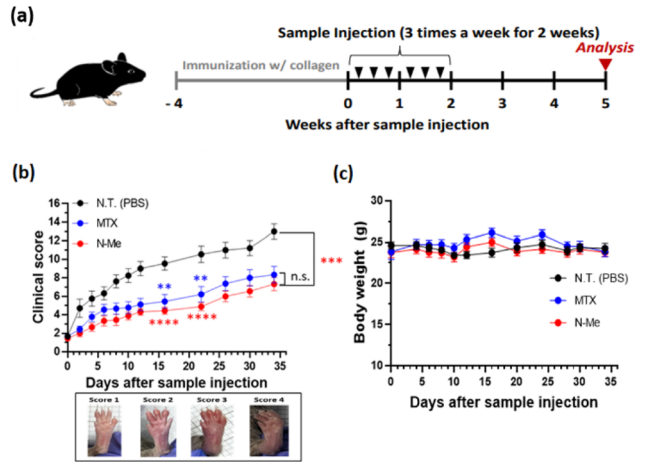

Fig. 5 Therapeutic Efficacy of N-Me in collagen-induced arthritis (CIA) model. (a) Overall experimental timeline for *in vivo* experiment with intraperitoneal injection 3 times a week for 2 weeks, and monitoring for 35 days after sample injection. (b) Representative images of paws with a corresponding clinical score of 1–4 and clinical score of CIA model mice treated with each sample (n = 9, Mean ± SD, $^{**}p < 0.01$, $^{***}p < 0.001$, $^{****}p < 0.0001$) and (c) bodyweight measurement (n = 9, Mean ± SD).

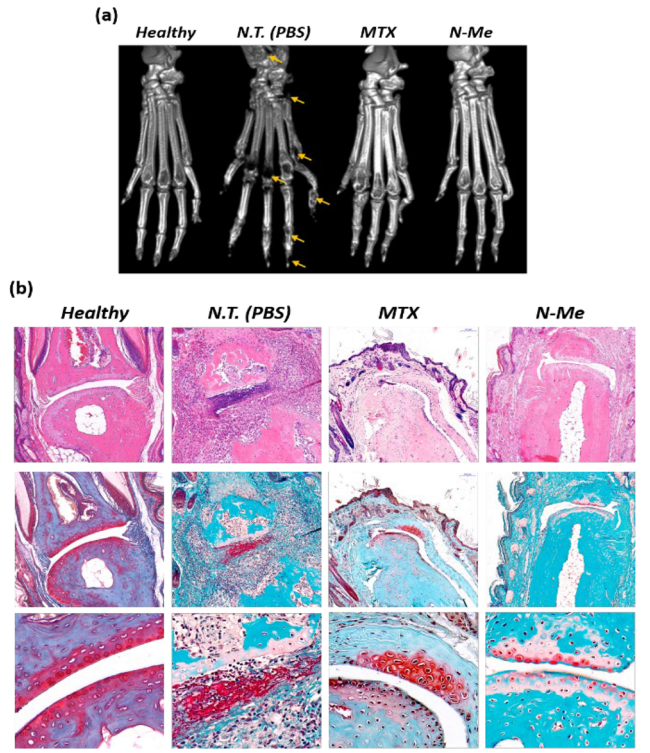

Fig. 6 *Ex vivo* study of the therapeutic efficacy of N-Me in CIA model mice. (a) Representative paw images of microcomputed tomography (micro-CT) images of healthy and CIA model mice. The yellow arrows indicate bone destruction and damage. (b) Images of hematoxylin and eosin (H&E) and safranin-O staining of representative joints in control and CIA mice (scale bars = 100 μm).

tion, leading to joint disorders.[43] Therefore, to investigate the degree of bone destruction, the paws of each group were monitored using CT. A significantly reduced bone density was observed in the PBS-treated group, which might be due to bone erosion in the ankles and finger joints. Although MTX has been known to reduce edema due to its inflammatory suppression effects, bone erosion was in progress, as shown by the destruction traces on the midfoot (Fig. 6a). Compared to that of PBS- and MTX-treated CIA mice, N-Me-treated CIA mice showed a significantly reduced degree of joint destruction, indicating clear ankle and finger joint boundaries and less bone erosion. H&E and safranin-O staining were performed to analyze the severity of edema, inflammation, and degree of cartilage damage. No infiltration or swelling of inflammatory cells was observed; however, clear cartilage was observed in the healthy group (Fig. 6b). In contrast, severe cartilage damage and inflammatory cell infiltration were observed in the PBS-treated group. In the N-Me-treated group, cartilage damage was insignificant, and the lack of infiltration of inflammatory cells around the joints was similar to that in the MTX-treated group. Thus, we confirmed the inhibitory effect on bone erosion and cartilage damage around joints in the N-Me-treated CIA mice through the protective effect of distinct joints by the NO-scavenging ability of N-Me.

3.8. Quantification of cytokines and NO level in CIA model

Since the main role of NO in RA is local immune response induction, we evaluated the pro-inflammatory cytokine levels

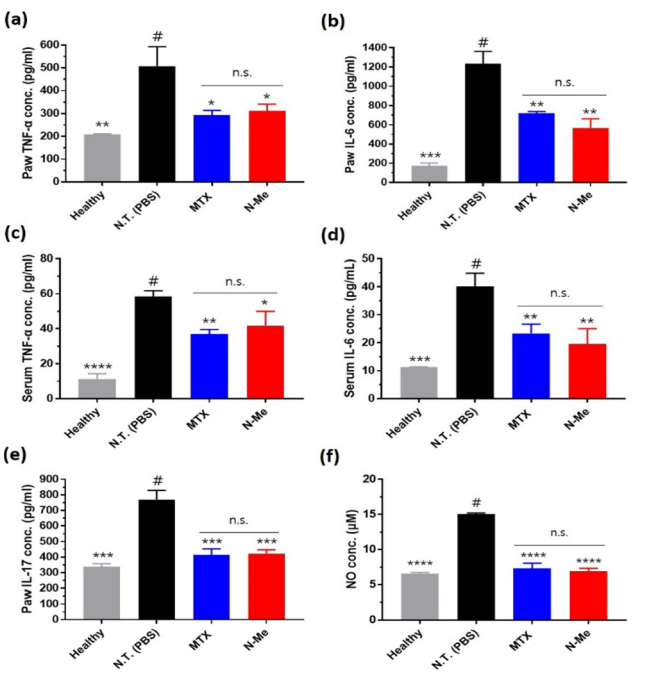

Fig. 7 *Ex vivo* cytokines and NO level in CIA model. The level of TNF-α, IL-6, and IL-17 were measured by ELISA in paw tissue fluid (a, b, and e) or serum (c and d). The level of NO were measured by Griess assay in paw tissue fluid (f) (n = 3, Mean ± SD, # compared with sample groups, $^{*}p < 0.05$, $^{**}p < 0.01$, $^{***}p < 0.001$, $^{****}p < 0.0001$).

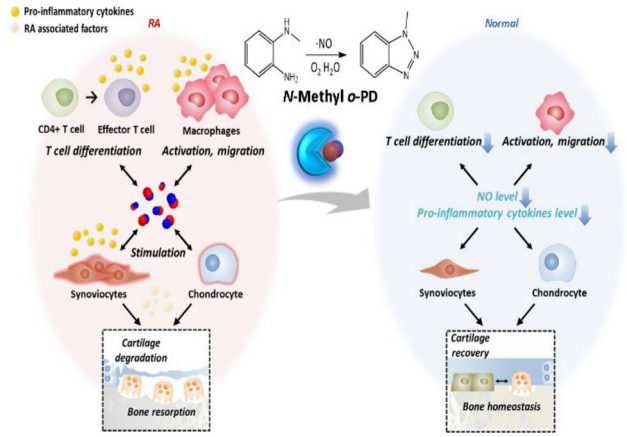

Scheme 2 A schematic illustration of N-Me as a potential for RA treatment by NO-scavenging.

in the tissue and serum *via* ELISA after the treatment of the samples *in vivo*. TNF-α and IL-6 were mainly expressed in macrophages and synoviocytes in RA,[44] and IL-17 produced in Th17 cells ($CD4^+$ T cell subset) helps osteoclasts to differentiate.[45] Overall, significantly reduced cytokine levels were observed in the N-Me-treated group and were similar to the inflammatory inhibitory effect of MTX (Fig. 7a–e). Since NO is a substance that induces COX-2, an inflammatory cytokine-producing mediator,[46] it is thought that inhibition of NO by N-Me is similar to the mechanism of MTX, which inhibits the same inflammatory mediator.[47] Finally, we measured the level of NO in the paw tissue. The level of NO in the joints in the N-Me-treated group was lower than that in the healthy group (Fig. 7f), indicating that NO was closely related to inflammation.

4. Conclusions

In this study, using a NO scavenger significantly reduced the immune responses in the RA lesion, leading to the alleviation of inflammation and joint recovery of RA. We discovered an *o*-PD-based NO scavenger that is highly reactive with NO as an agent for RA treatment. Through the NO-scavenging fluorescence assay, it was confirmed that modification of amine in *o*-PD can contribute to increasing its reactivity with NO. This is the first case of RA treatment using only a small-molecule NO scavenger, without any additional combination. We believe that the discovery of N-Me with improved reactivity with NO in this study has potential applications for developing anti-inflammatory disease treatments targeting NO (Scheme 2).

Author contributions

The study was designed by S. L., Y. M. L. and W. J. K., and performed all experiments and analyzed the data by S. L. and Y. M. L., supervised the overall research by Y. M. L. and W. J. K. The manuscript was written by S. L. and Y. M. L. and revised by Y. M. L., S. L. and W. J. K.

Conflicts of interest

W. J. K. is the CEO of the OmniaMed, but declares no conflict of interest for this paper.

Acknowledgements

This work was supported by the National Research Foundation of Korea (NRF) Grant (NRF-2022R1A3B1077354) and the Creative Materials Discovery Program (NRF-2018M3D1A1058813) funded by the Korea government (Ministry of Science and ICT).

References

1 J. S. Smolen and D. Aletaha, Rheumatoid arthritis, *Nat. Rev. Dis. Primers*, 2018, **4**, 18001.
2 A. Damerau and T. Gaber, Modeling rheumatoid arthritis in vitro: From experimental feasibility to physiological proximity, *Int. J. Mol. Sci.*, 2020, **21**, 7916.
3 Rheumatoid Arthritis: Global Drug Forecast and Market Analysis to 2029.
4 M. Mellado, *et al.*, T cell migration in rheumatoid arthritis, *Front. Immunol.*, 2015, **6**, 384.
5 M. S. Akram, N. Pery, *et al.*, Challenges for biosimilars: focus on rheumatoid arthritis, *Crit. Rev. Biotechnol.*, 2021, **41**, 121–153.
6 P. Geusens, The role of RANK ligand/osteoprotegerin in rheumatoid arthritis, *Ther. Adv. Musculoskeletal Dis.*, 2012, **4**, 225–233.
7 P. Suresh, *et al.*, Development of a Novel Methotrexate-Loaded Nanoemulsion for Rheumatoid Arthritis Treatment with Site-Specific Targeting Subcutaneous Delivery, *Nanomaterials*, 2022, **12**, 1299.
8 M. Maciejewski, *et al.*, Prediction of response of methotrexate in patients with rheumatoid arthritis using serum lipidomics, *Sci. Rep.*, 2021, **11**, 1–6.
9 L. Fraenkel, *et al.*, 2021 American College of Rheumatology guideline for the treatment of rheumatoid arthritis, *Arthritis Rheumatol.*, 2021, **73**, 1108–1123.
10 JAK Inhibitors for Rheumatoid Arthritis By Elizabeth Svoboda Medically Reviewed by Brunilda Nazario, MD on October 07, 2021.
11 A. Schwentker and T. R. Billiar, Inducible nitric oxide synthase: from cloning to therapeutic applications, *World J. Surg.*, 2002, **26**, 772.
12 B. Lima, *et al.*, S-nitrosylation in cardiovascular signaling, *Circ. Res.*, 2010, **106**, 633–646.
13 P. Tripathi, *et al.*, The role of nitric oxide in inflammatory reactions, *FEMS Immunol. Med. Microbiol.*, 2007, **51**, 443–452.

14 R. J. Van't Hof, *et al.*, Nitric oxide is a mediator of apoptosis in the rheumatoid joint, *Rheumatology*, 2000, **39**, 1004–1008.
15 W. Niedbala, *et al.*, Nitric oxide preferentially induces type 1 T cell differentiation by selectively up-regulating IL-12 receptor β2 expression via cGMP, *Proc. Natl. Acad. Sci. U. S. A.*, 2002, **99**, 16186–16191.
16 W.-J. Gao, *et al.*, Suppression of macrophage migration by down-regulating Src/FAK/P130Cas activation contributed to the anti-inflammatory activity of sinomenine, *Pharmacol. Res.*, 2021, **167**, 105513.
17 M.-C. Maa, *et al.*, Requirement of inducible nitric-oxide synthase in lipopolysaccharide-mediated Src induction and macrophage migration, *J. Biol. Chem.*, 2008, **283**, 31408–31416.
18 F. Spiller, *et al.*, Targeting nitric oxide as a key modulator of sepsis, arthritis and pain, *Nitric Oxide*, 2019, **89**, 32–40.
19 S. R. Goldrin, *et al.*, The role of cytokines in cartilage matrix degeneration in osteoarthritis, *Clin. Orthop. Relat. Res.*, 2004, **427**, S27–S36.
20 A. R. Amin, M. Attur, *et al.*, Nitric oxide synthase and cyclooxygenases: distribution, regulation, and intervention in arthritis, *Curr. Opin. Rheumatol.*, 1999, **11**, 202–209.
21 K. Fuller, *et al.*, TRANCE is necessary and sufficient for osteoblast-mediated activation of bone resorption in osteoclasts, *J. Exp. Med.*, 1998, **188**, 997–1001.
22 H. Yasuda, *et al.*, Osteoclast differentiation factor is a ligand for osteoprotegerin/osteoclastogenesis-inhibitory factor and is identical to TRANCE/RANKL, *Proc. Natl. Acad. Sci. U. S. A.*, 1998, **95**, 3597–3602.
23 D. L. Lacey, *et al.*, Osteoprotegerin ligand is a cytokine that regulates osteoclast differentiation and activation, *Cell*, 1998, **93**, 165–176.
24 D. Salvemini, S. F. Kim and V. Mollace, Reciprocal regulation of the nitric oxide and cyclooxygenase pathway in pathophysiology: relevance and clinical implications, *Am. J. Physiol.: Regul., Integr. Comp. Physiol.*, 2013, **4**, R473–R487.
25 M. A. Marletta, Approaches toward selective inhibition of nitric oxide synthase, *J. Med. Chem.*, 1994, **37**, 1899–1907.
26 D. D. Davey, *et al.*, Design, synthesis, and activity of 2-imidazol-1-ylpyrimidine derived inducible nitric oxide synthase dimerization inhibitors, *J. Med. Chem.*, 2007, **50**, 1146–1157.
27 R. Korhonen, *et al.*, Dexamethasone inhibits inducible nitric-oxide synthase expression and nitric oxide production by destabilizing mRNA in lipopolysaccharide-treated macrophages, *Mol. Pharmacol.*, 2002, **62**, 698–704.
28 S. Tao, *et al.*, Breathing micelles for combinatorial treatment of rheumatoid arthritis, *Angew. Chem., Int. Ed.*, 2020, **59**, 21864–21869.
29 J. Yeo, Y. M. Lee, *et al.*, Nitric oxide-scavenging nanogel for treating rheumatoid arthritis, *Nano Lett.*, 2019, **19**, 6716–6724.
30 T. Kim, J. Suh and W. J. Kim, Polymeric Aggregate–Embodied Hybrid Nitric–Oxide–Scavenging and Sequential Drug–Releasing Hydrogel for Combinatorial Treatment of Rheumatoid Arthritis, *Adv. Mater.*, 2021, **33**, 2008793.
31 C. Ley, *et al.*, *Ullmann's encyclopedia of industrial chemistry*, Wiley, Chichester, UK, 2010.
32 *Vogel's Textbook of Practical Organic Chemistry* by B. S. Furniss, A. J. Hannaford, P. W. G. Smith and A. R. Tatchell, 5th edn, 1989, p. 1163.
33 Y. Huo, *et al.*, Aromatic primary monoamine-based fast-response and highly specific fluorescent probes for imaging the biological signaling molecule nitric oxide in living cells and organisms, *J. Mater. Chem. B*, 2017, **5**, 2483–2490.
34 J. Park, *et al.*, Therapeutic–Gas–Responsive Hydrogel, *Adv. Mater.*, 2017, **29**, 1702859.
35 M. Finšgar, *et al.*, Inhibition of copper corrosion by 1, 2, 3-benzotriazole: a review, *Corros. Sci.*, 2010, **52**, 2737–2749.
36 T.-W. Shiue, *et al.*, Nitric oxide turn-on fluorescent probe based on deamination of aromatic primary monoamines, *Inorg. Chem.*, 2012, **51**, 5400–5408.
37 Y. Huo, *et al.*, Aromatic primary monoamine-based fast-response and highly specific fluorescent probes for imaging the biological signaling molecule nitric oxide in living cells and organisms, *J. Mater. Chem. B*, 2017, **5**, 2483–2490.
38 S. Roychowdhury, A. Luthe, *et al.*, Oxidative stress in glial cultures: detection by DAF–2 fluorescence used as a tool to measure peroxynitrite rather than nitric oxide, *Glia*, 2002, **38**, 103–114.
39 Y. Huo, *et al.*, Aromatic primary monoamine-based fast-response and highly specific fluorescent probes for imaging the biological signaling molecule nitric oxide in living cells and organisms, *J. Mater. Chem. B*, 2017, **5**, 2483–2490.
40 K. T. Savjani, A. K. Gajjar and J. K. Savjani, Drug solubility: importance and enhancement techniques, *ISRN Pharmacol.*, 2012, **2012**, 195727.
41 Y. W. Su, W. F. Chiou, *et al.*, Ligustilide prevents LPS-induced iNOS expression in RAW 264.7 macrophages by preventing ROS production and down-regulating the MAPK, NF-κB and AP-1 signaling pathways, *Int. Immunopharmacol.*, 2011, **11**, 1166–1172.
42 D. D. Brand, K. A. Latham, *et al.*, Collagen-induced arthritis, *Nat. Protoc.*, 2007, **2**, 1269–1275.
43 C. Liu, Y. Zhang, *et al.*, Triptolide prevents bone destruction in the collagen-induced arthritis model of rheumatoid arthritis by targeting RANKL/RANK/OPG signal pathway, *Evidence-Based Complementary Altern. Med.*, 2013, 1–12.
44 I. B. McInnes, C. D. Buckley and J. D. Isaacs, Cytokines in rheumatoid arthritis—shaping the immunological landscape, *Nat. Rev. Rheumatol.*, 2016, **12**, 63–68.
45 D. Lin, *et al.*, Interleukin–17 regulates the expressions of RANKL and OPG in human periodontal ligament cells via TRAF 6/TBK 1—JNK/NF–κB pathways, *Immunology*, 2015, **144**, 472–485.

46 V. Mollace, *et al.*, Modulation of prostaglandin biosynthesis by nitric oxide and nitric oxide donors, *Pharmacol. Rev.*, 2005, **57**, 217–252.

47 S. B. V. Mello, D. M. Barros, *et al.*, Methotrexate as a preferential cyclooxygenase 2 inhibitor in whole blood of patients with rheumatoid arthritis, *Rheumatology*, 2000, **39**, 533–536.